Single-photon superradiance and radiation trapping by atomic shells

Anatoly A. Svidzinsky,[1,2] Fu Li,[1] Hongyuan Li,[1,3] Xiwen Zhang,[1] C. H. Raymond Ooi,[4] and Marlan O. Scully[1,2,5]

[1]*Texas A&M University, College Station, Texas 77843, USA*
[2]*Princeton University, Princeton, New Jersey 08544, USA*
[3]*Xi'an Jiaotong University, Xi'an, China*
[4]*University of Malaya, 50603 Kuala Lumpur, Malaysia*
[5]*Baylor University, Waco, Texas 76706, USA*

The collective nature of light emission by atomic ensembles yields fascinating effects such as superradiance and radiation trapping even at the single-photon level. Light emission is influenced by virtual transitions and the collective Lamb shift which yields peculiar features in temporal evolution of the atomic system. We study how two-dimensional atomic structures collectively emit a single photon. Namely, we consider spherical, cylindrical, and spheroidal shells with two-level atoms continuously distributed on the shell surface and find exact analytical solutions for eigenstates of such systems and their collective decay rates and frequency shifts. We identify states which undergo superradiant decay and states which are trapped and investigate how size and shape of the shell affects collective light emission. Our findings could be useful for quantum information storage and the design of optical switches.

I. INTRODUCTION

Collective spontaneous emission from atomic ensembles has been a subject of long-standing interest since the pioneering work of Dicke [1]. If a single photon is stored in the atomic cloud (and shared among many atoms) the state undergoes collective spontaneous decay which could be superradiant if the atoms are properly phased. The rate of spontaneous emission can be enhanced or inhibited by changing the density of optical modes into which the photon is emitted [2,3]. This can be effectively achieved, e.g., by placing atoms in a microcavity [4–6].

Virtual (off-resonance) photons are a fascinating aspect of quantum electrodynamics. In contrast to real photons, which may be detected, their virtual counterparts have a fleeting existence limited by the time-energy uncertainty relation. Virtual photons exist in and only in the interaction and they do not generally conserve energy and momentum. The emission and the subsequent absorption of one or more virtual photons, however, give rise to measurable effects. For example, the Lamb shift [7] arises from a modification of the transition frequency of an atom due to the emission and reabsorption of transverse virtual photons. In quantum field theory, even classical forces, such as the Coulomb repulsion or attraction between two charges, can be thought of as due to the exchange of timelike virtual photons between the charges [8]. By modulating the atom-field coupling strength, virtual photons can be released as a form of quantum vacuum radiation [9].

Virtual transitions have interesting effects on the collective emission of atoms [10–12]. In particular, if the initial atomic state is superradiant the virtual transitions partially transfer population into slowly decaying states which results in a trapping of some amount of atomic excitation. On the other hand, for slowly decaying states virtual processes yield additional decay channels which leads to a slow decay of the otherwise trapped states. Virtually exchanging off-resonant photons also induce a collective Lamb shift [13–19].

One should note that quantization of the electromagnetic field in the Coulomb gauge yields only transverse photons. On the other hand, field quantization in the Lorenz gauge also gives timelike and longitudinal photons [8]. The abovementioned references on the collective Lamb shift, as well as the present paper, use the Coulomb gauge and, thus, the Lamb shift appears to be due to the exchange of virtual off-resonance transverse photons.

A photon propagating through an extended atomic cloud is collectively absorbed and reemitted which yields collective oscillations of the field envelope [20,21]. Such collective oscillations can be amplified by a low-frequency coherent drive by a mechanism of the difference combination resonance which leads to generation of high-frequency coherent radiation [22].

Many-photon superradiance has been observed experimentally in various systems, e.g., in optically pumped HF gas [23], helium plasma [24], and Cs atoms trapped in the near field of a photonic crystal waveguide [25]. Superradiance has been also discussed for excitons in semiconductors. In a crystal, the exciton can interact with a photon forming the polariton, i.e., a hybridized mode of exciton and photon. Since the exciton is a coherent elementary excitation over the whole crystal it can decay superradiantly through its macroscopic transition dipole moment [26]. Exciton superradiance in crystal slabs has been studied in Refs. [27,28]. It was demonstrated that superradiance can be treated by a unified formalism for atoms, Frenkel and Wannier excitons [28]. A crossover from two-dimensional to three-dimensional crystals was investigated in Ref. [29]. A nonlocal theory of the collective radiative decay of excitons was developed for semiconductor quantum dots [30] and spherical semiconductor nanocrystals [31]. A transition between the strong (coherent) and weak (incoherent) coupling limits of interaction between quantum well excitons and bulk photons was analyzed in Ref. [32]. Exciton-photon coupled modes in a semiconductor film were investigated theoretically in Ref. [33]. Exciton superradiance in semiconductor microcrystals of CuCl was observed in Ref. [34].

Recent studies focus on collective, virtual, and nonlocal effects in atomic [11,12,16,21,35–63] and nuclear [16,64–69] ensembles. A short while ago it was shown that quantum

mechanical evolution equations for probability amplitudes that describe single-photon emission (absorption) by atomic ensembles can be written in a form equivalent to the semiclassical Maxwell-Bloch equations [70]. This connection allows us to considerably simplify the fully quantum mechanical treatment of the problem and find new analytical solutions.

Cooperative spontaneous emission can provide insights into quantum electrodynamics and is important for various applications of the entangled atomic ensembles and generated quantum states of light for quantum memories [71–77], quantum cryptography [78,79], quantum communication [43,73,80], and quantum information [43,47]. Superradiance also has important applications for realizing single-photon sources [81,82], laser cooling by way of cooperative emission [83,84], and narrow linewidth lasers [85]. Collective interaction of light with nuclei arrays can be also used to control propagation of γ rays on a short (superradiant) time scale [86].

In nature there exist two-dimensional atomic structures with unique properties. One example is graphene which is an allotrope of carbon in the form of a two-dimensional, atomic scale, hexagonal lattice. It is the basic structural element of graphite, charcoal, carbon nanotubes, and fullerenes. Nitrogen vacancy centers on the surface of bulk diamonds is another interesting example of a two-dimensional shell structure geometry. Nitrogen vacancy (NV) centers are point defects in the diamond lattice which are typically produced by diamond irradiation followed by annealing. The NV can be controlled coherently at room temperature using electromagnetic fields. Due to its energy level structure, NV fluorescence is spin-state dependent, allowing simple routes for optical initialization and readout. For these reasons, the NV center is one of the most prominent candidates for room temperature quantum information processing.

Here we investigate how two-dimensional atomic structures collectively emit light. Namely, we study spherical, cylindrical, and spheroidal shells with two-level atoms continuously distributed on the shell surface (see Fig. 1). We find eigenstates of such systems and their collective decay rates and collective frequency (Lamb) shifts. One should mention that eigenstates
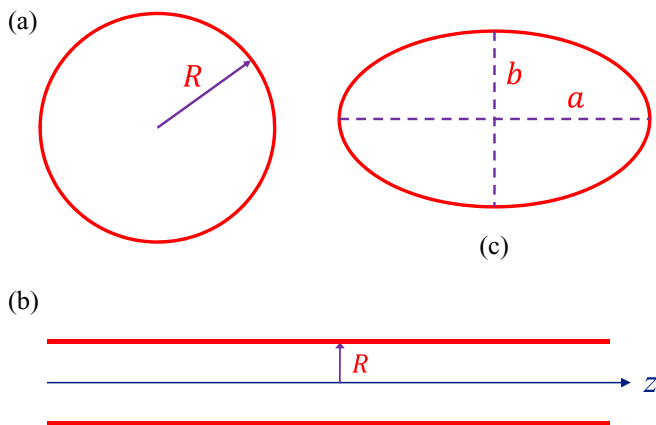

FIG. 1. Geometry of atomic shells: Atoms are continuously distributed on a surface of a sphere (a), an infinitely long cylinder (b), or a spheroid (c).

for various bulk geometries when atoms occupy the interior of a sphere [12,38,39,42,87], cylinder [88–90], slab [40], or multislice slab configuration [91] have been studied in the literature. Collective exciton states in a core-shell microsphere have been investigated in Ref. [92]. However, as we show, for the shell atomic structures which we study here the problem has exact analytical solutions. Such solutions yield new interesting insights on the collective single-photon emission and show under what conditions the atoms undergo fast superradiant decay and when collective excitation is trapped (does not decay even in the presence of virtual transitions).

In this paper we study collective photon emission by an ensemble of two-level ($|a\rangle$ excited and $|b\rangle$ ground state) atoms with spacing between levels $E_a - E_b = \hbar\omega$. For a dense cloud of volume V, the evolution of an atomic system in a scalar photon theory is described by an integral equation with an exponential kernel [12,38,39]:

$$\frac{\partial \beta(t,\mathbf{r})}{\partial t} = i\gamma \int d\mathbf{r}' n(\mathbf{r}') \frac{\exp(ik_0|\mathbf{r} - \mathbf{r}'|)}{k_0|\mathbf{r} - \mathbf{r}'|} \beta(t,\mathbf{r}'), \quad (1)$$

where $\beta(t,\mathbf{r})$ is the probability amplitude to find the atom at position $\mathbf{r}$ excited at time t, γ is the single-atom decay rate, $k_0 = \omega/c$ is the wave number associated with the atomic transition, and $n(\mathbf{r})$ is the atomic density. Equation (1) takes into account virtual (off-resonance) processes and is valid in the Markovian (local) approximation in which the evolution of the system at time t depends only on the state of the system at this moment of time. This is a good approximation provided that the characteristic time scale of the system evolution is longer than the time of photon flight through the atomic cloud. However, if the size of the sample is large enough, the local approximation breaks down and the system's dynamics becomes nonlocal in time. The generalization of Eq. (1) including retardation effects has been considered in Ref. [57].

The eigenfunctions of Eq. (1),

$$\beta(t,\mathbf{r}) = e^{-\Gamma t}\beta(\mathbf{r}), \quad (2)$$

and eigenvalues Γ determine the evolution of the atomic system. The real part of Γ yields the state decay rate, while Im(Γ) describes the frequency (Lamb) shift of the collective excitation. The eigenfunction equation for $\beta(\mathbf{r})$ reads

$$-i\gamma \int d\mathbf{r}' n(\mathbf{r}') \frac{\exp(ik_0|\mathbf{r} - \mathbf{r}'|)}{k_0|\mathbf{r} - \mathbf{r}'|} \beta(\mathbf{r}') = \Gamma\beta(\mathbf{r}). \quad (3)$$

Next we investigate solutions of Eq. (3) for various shelllike structures.

II. SPHERICAL SHELL

In this section we consider a spherical shell of radius R [see Fig. 1(a)]. Atoms are continuously distributed over the sphere surface. In spherical coordinates $\mathbf{r} = (r,\theta,\phi)$ the atomic density is $n(\mathbf{r}) = N\delta(r - R)/4\pi R^2$, where N is the total number of atoms in the shell. For such geometry Eq. (3) reads

$$-\frac{i\gamma N}{4\pi} \int d\Omega_{r'} \frac{\exp(ik_0 R|\hat{r} - \hat{r}'|)}{k_0 R|\hat{r} - \hat{r}'|} \beta(\hat{r}') = \Gamma\beta(\hat{r}), \quad (4)$$

where $\hat{r}$ is a unit vector in the direction of $\mathbf{r}$ and integration is performed over all angles. We look for the solution of Eq. (4)

in the form

$$\beta(\hat{r}) = Y_{nm}(\hat{r}), \tag{5}$$

where $Y_{nm}(\hat{r}) \equiv Y_{nm}(\theta, \varphi)$ are spherical harmonics. Substituting this into Eq. (4) we obtain the following equation for the eigenvalues Γ:

$$-\frac{i\gamma N}{4\pi} \int d\Omega_{r'} \frac{\exp(ik_0 R |\hat{r} - \hat{r}'|)}{k_0 R |\hat{r} - \hat{r}'|} Y_{nm}(\hat{r}') = \Gamma Y_{nm}(\hat{r}). \tag{6}$$

Next we use the expansion

$$\frac{\exp(ik_0 R |\hat{r} - \hat{r}'|)}{k_0 R |\hat{r} - \hat{r}'|}$$
$$= 4\pi i \sum_{k=0}^{\infty} \sum_{s=-k}^{k} Y_{ks}(\hat{r}) Y_{ks}^*(\hat{r}') j_k(k_0 R) h_k^{(1)}(k_0 R), \tag{7}$$

where $\hat{r}$ and $\hat{r}'$ are unit vectors in the directions of $\mathbf{r}$ and $\mathbf{r}'$, respectively, and $j_k(z)$ and $h_k^{(1)}(z)$ are the spherical Bessel and Hankel functions. The substitution of Eq. (7) into Eq. (6) yields

$$\gamma N \sum_{k=0}^{\infty} \sum_{s=-k}^{k} Y_{ks}(\hat{r}) j_k(k_0 R) h_k^{(1)}(k_0 R)$$
$$\times \int d\Omega_{r'} Y_{ks}^*(\hat{r}') Y_{nm}(\hat{r}') = \Gamma Y_{nm}(\hat{r}). \tag{8}$$

One can perform integration over $\mathbf{r}'$ directions in Eq. (8) using the orthogonality condition for spherical harmonics,

$$\int d\Omega_{r'} Y_{ks}^*(\hat{r}') Y_{nm}(\hat{r}') = \delta_{nk} \delta_{sm}, \tag{9}$$

which gives the following answer for the eigenvalues:

$$\Gamma_n = N\gamma j_n(k_0 R) h_n^{(1)}(k_0 R). \tag{10}$$

For the spherical shell geometry each eigenvalue is $(2n+1)$-fold degenerate.

Spherical Hankel functions can be written as a combination of the spherical Bessel functions of the first and the second kind as

$$h_n^{(1)}(x) = j_n(x) + i y_n(x). \tag{11}$$

Thus, the real and imaginary parts of the eigenvalues are

$$\mathrm{Re}(\Gamma_n) = N\gamma j_n^2(k_0 R), \tag{12}$$

$$\mathrm{Im}(\Gamma_n) = N\gamma j_n(k_0 R) y_n(k_0 R). \tag{13}$$

For small atomic shell $k_0 R \ll 1$, Eqs. (12) and (13) yield

$$\mathrm{Re}(\Gamma_n) \approx N\gamma \frac{(k_0 R)^{2n}}{[(2n+1)!!]^2}, \tag{14}$$

$$\mathrm{Im}(\Gamma_n) \approx -\frac{N\gamma}{(2n+1)} \frac{1}{k_0 R}, \tag{15}$$

while in the large sample limit $k_0 R \gg 1$ we obtain

$$\mathrm{Re}(\Gamma_n) \approx N\gamma \frac{\sin^2(k_0 R - \pi n/2)}{(k_0 R)^2}, \tag{16}$$

$$\mathrm{Im}(\Gamma_n) \approx -N\gamma \frac{\sin(2k_0 R - \pi n)}{2(k_0 R)^2}. \tag{17}$$

For the spherically symmetric eigenstate $n = 0$, Eqs. (12) and (13) reduce to

$$\mathrm{Re}(\Gamma_0) = N\gamma \frac{\sin^2(k_0 R)}{(k_0 R)^2}, \tag{18}$$

$$\mathrm{Im}(\Gamma_0) = -N\gamma \frac{\sin(2k_0 R)}{2(k_0 R)^2}. \tag{19}$$

Equation (18) shows that a spherically symmetric state with $n = 0$ has the fastest decay rate,

$$\mathrm{Re}(\Gamma_0) = N\gamma, \tag{20}$$

in the small sample limit $k_0 R \ll 1$. However, the collective Lamb shift for such a state is very large and is given by $\mathrm{Im}(\Gamma_0) = -N\gamma/k_0 R$ in this limit.

On the other hand, states for which

$$k_0 R = A_{nl}, \tag{21}$$

where A_{nl} are zeros of the spherical Bessel function $j_n(x)$, are trapped. For such states $\mathrm{Re}(\Gamma) = 0$. The collective Lamb shift for such states also vanishes. In particular, for $n = 0$ we obtain that the state is trapped for

$$k_0 R = \pi l, \tag{22}$$

where $l = 1, 2, 3, \ldots$.

State trapping can be understood as follows. Maxwell's equations for the electromagnetic field have the following normal modes in spherical coordinates:

$$E(r, \theta, \phi) = E_0 j_n(k_0 r) Y_{nm}(\hat{r}). \tag{23}$$

If for $r = R$ the electric field in the mode vanishes then such a mode is not coupled with the atomic spherical shell of radius R. This is the case if the spherical Bessel function $j_n(x)$ has a zero at $x = k_0 R$. As a result atoms in the state $Y_{nm}(\hat{r})$ cannot emit photons into this mode and the state does not decay even in the presence of virtual transitions.

By changing the radius of the spherical shell one can control how fast the state decays. As a demonstration, in Fig. 2 we plot
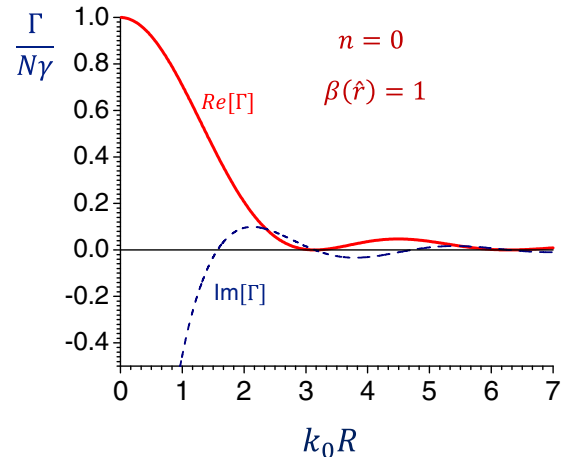

FIG. 2. Collective decay rate (red solid line) and frequency shift (blue dash line) of a spherical atomic shell as a function of the radius of the sphere R. Initially atoms are prepared in the symmetric state $\beta(\mathbf{r}) = 1$.
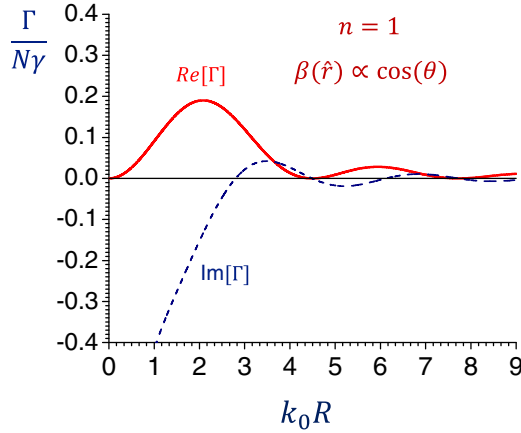
FIG. 3. The same as in Fig. (2) but for the initial eigenstate $\beta(\mathbf{r}) = \cos(\theta)$.

the collective decay rate (red solid line) and the frequency shift (blue dash line) of a spherical atomic shell as a function of the radius of the sphere R for the symmetric eigenstate $\beta(\mathbf{r}) = 1$. For the small shell radius $k_0 R \ll 1$ the state undergoes superradiant decay with the rate $N\gamma$. However, when $k_0 R = \pi, 2\pi, \ldots$, the symmetric state is trapped and the decay rate is equal to zero.

In Fig. 3 we plot the collective decay rate (red solid line) and the frequency shift (blue dash line) as a function of the radius of the sphere R for the first spherical harmonic $\beta(\mathbf{r}) = \cos(\theta)$ ($n = 1, m = 0$). For a small shell such a state is trapped. However, it becomes superradiant if we increase the shell size. The decay rate for such a state is maximum for $k_0 R = 2.08$ and is equal to $0.19 N\gamma$.

In Fig. 4 we plot the decay rate of several spherical harmonics $\beta(\mathbf{r}) = Y_{nm}(\theta, \phi)$ ($n = 0, 1, 2, 3$) as a function of the radius of the sphere R. For each spherical harmonic there is a range of the shell radii for which such a harmonic has the fastest decay rate. Thus, if we want to make atoms decay fast for a certain radius of the sphere we must prepare the state of the sample to be a particular spherical harmonic.
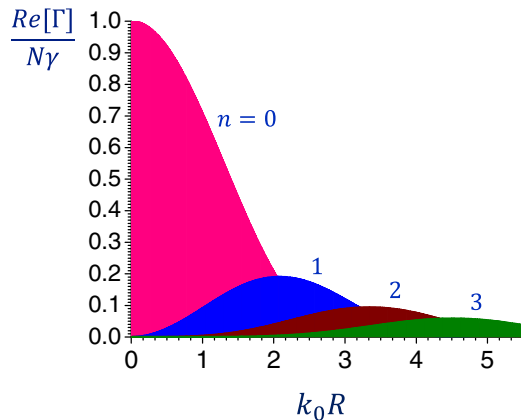

FIG. 4. Decay rate of spherical harmonics $\beta(\mathbf{r}) = Y_{nm}(\theta, \phi)$ ($n = 0, 1, 2, 3$) of a spherical atomic shell as a function of the radius of the sphere R.

Finally we discuss the collective decay of an atomic state prepared by absorption of a plane-wave photon with the wave vector $\mathbf{k}_0$. We assume that the initial state of the atoms is

$$\beta(0, \mathbf{r}) = \frac{1}{\sqrt{4\pi}} e^{i\mathbf{k}_0 \cdot \mathbf{r}}, \tag{24}$$

where $\mathbf{r} = R\hat{r}$. Expanding the initial state into eigenstates (5) (spherical harmonics) we obtain

$$\beta(0, \mathbf{r}) = \sqrt{4\pi} \sum_{n=0}^{\infty} \sum_{m=-n}^{n} i^n j_n(k_0 R) Y_{nm}^*(\hat{k}_0) Y_{nm}(\hat{r}), \tag{25}$$

where $\hat{k}_0$ is a unit vector in the direction of $\mathbf{k}_0$. Evolution of the initial state (24) is given by

$$\beta(t, \mathbf{r}) = \sqrt{4\pi} \sum_{n=0}^{\infty} \sum_{m=-n}^{n} i^n j_n(k_0 R) Y_{nm}^*(\hat{k}_0) Y_{nm}(\hat{r}) e^{-\Gamma_n t}, \tag{26}$$

where Γ_n is the eigenvalue corresponding to the eigenstate $Y_{nm}(\hat{r})$. We calculate the probability $P(t)$ that atoms in the shell are excited as a function of time:

$$P(t) = \int |\beta(t, \mathbf{r})|^2 d\Omega_r, \tag{27}$$

where integration is over the solid angle. Using Eq. (26) and taking into account the orthogonality condition for spherical harmonics (9) we obtain

$$P(t) = 4\pi \sum_{n=0}^{\infty} \sum_{m=-n}^{n} j_n^2(k_0 R) Y_{nm}^*(\hat{k}_0) Y_{nm}(\hat{k}_0) e^{-2\mathrm{Re}(\Gamma_n)t}. \tag{28}$$

Finally using Unsöld's theorem

$$\sum_{m=-n}^{n} Y_{nm}^*(\hat{k}_0) Y_{nm}(\hat{k}_0) = \frac{2n+1}{4\pi} \tag{29}$$

and expression for the eigenvalues (12) we find

$$P(t) = \sum_{n=0}^{\infty} (2n+1) j_n^2(k_0 R) e^{-2N\gamma j_n^2(k_0 R)t}. \tag{30}$$

Since

$$\sum_{n=0}^{\infty} (2n+1) j_n^2(k_0 R) = 1 \tag{31}$$

at the initial moment of time $P(0) = 1$; that is, $P(t)$ is properly normalized.

In Fig. 5 we plot $P(t)$ given by Eq. (30) for different radii of the spherical shell $k_0 R = 0.1, 1, 2, 3$, and 5. The vertical axis has a logarithmic scale and, thus, an exponentially decaying function would appear as a straight line. Figure 5 illustrates that for $k_0 R \ll 1$ the state decays exponentially with the rate $N\gamma$ until the probability to find atoms excited becomes small. On the other hand, for $k_0 R \gtrsim 1$ the decay is not exponential because in this limit the initial state overlaps with many eigenstates of the system. The decay of atoms is now much slower. In Fig. 6 we plot $P(t)$ for a very large shell size, namely, $k_0 R = 10$. In this case the nonexponential decay
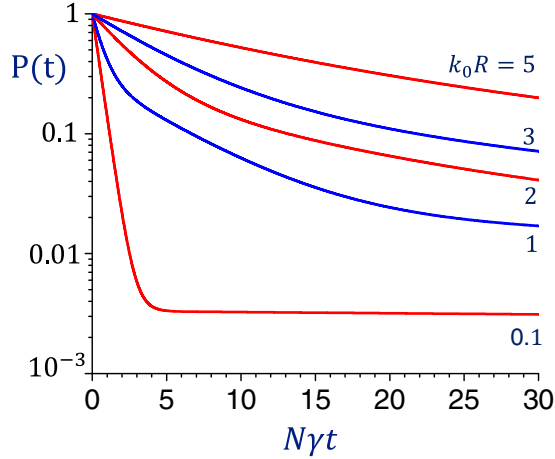
FIG. 5. Probability to find atoms excited as a function of time for different radii of the spherical shell. Initially atoms are prepared in the state (24). The vertical axis has a logarithmic scale.

of the initial state becomes very pronounced.

III. CYLINDRICAL SHELL

In this section we consider the infinitely long cylindrical shell of radius R [Fig. 1(b)] and use the cylindrical coordinates $\mathbf{r} = (\rho, \varphi, z)$. Atoms are continuously distributed on the cylinder surface with the density $n(\mathbf{r}) = n_0 \delta(\rho - R)/2\pi R$, where n_0 is the number of atoms per unit length of the cylinder. For such geometry, eigenfunction equation (3) reads

$$-\frac{i\gamma n_0}{2\pi k_0} \int_0^{2\pi} d\varphi' \int_{-\infty}^{\infty} dz' K(\varphi - \varphi', z - z')\beta(\varphi', z') = \Gamma \beta(\varphi, z),$$

(32)

where

$$K(\varphi, z) = \frac{\exp[ik_0\sqrt{2R^2 - 2R^2\cos(\varphi) + z^2}]}{\sqrt{2R^2 - 2R^2\cos(\varphi) + z^2}}.$$
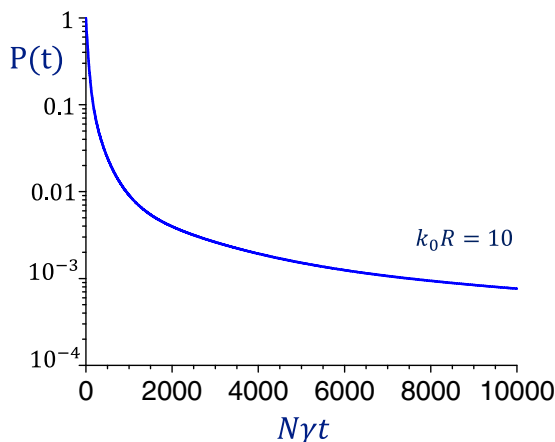
(33)

FIG. 6. The same as in Fig. 5 but for $k_0 R = 10$.

To find eigenfunctions and eigenvalues of the integral equation (32) we use the following expansion

$$K(\varphi, z) = \frac{i}{2} \int_{-\infty}^{\infty} dk \sum_{m=-\infty}^{\infty} J_m\left(\sqrt{k_0^2 - k^2}R\right)$$
$$\times H_m^{(1)}\left(\sqrt{k_0^2 - k^2}R\right)e^{ikz}e^{im\varphi},$$

(34)

where $J_m(x)$ and $H_m^{(1)}(x)$ are the Bessel and Hankel functions of the first kind. We look for the solution of Eq. (32) in the form

$$\beta(\varphi, z) = e^{in\varphi}e^{ik_z z},$$

(35)

where n is an integer number and k_z is the wave number of the mode along the cylindrical axis z. Substituting this into Eq. (32), using Eq. (34) and

$$\int_{-\infty}^{\infty} dz e^{i(k_z - k)z} = 2\pi \delta(k - k_z),$$

(36)

$$\int_0^{2\pi} d\varphi' e^{i(n-m)\varphi'} = 2\pi \delta_{nm},$$

(37)

we obtain the following expression for the eigenvalues Γ:

$$\Gamma = \frac{\pi \gamma n_0}{k_0} J_n\left(\sqrt{k_0^2 - k_z^2}R\right)H_n^{(1)}\left(\sqrt{k_0^2 - k_z^2}R\right).$$

(38)

For $k_z \leqslant k_0$ it is convenient to write the Hankel functions as a combination of the Bessel functions of the first and the second kind:

$$H_n^{(1)}(x) = J_n(x) + iY_n(x).$$

(39)

On the other hand, for $k_z > k_0$ we use the relations $J_n(ix) = i^n I_n(x)$ and $H_n^{(1)}(ix) = 2K_n(x)/\pi i^{n+1}$, where $I_n(x)$ and $K_n(x)$ are the modified Bessel functions of the first and the second kind. This yields the following answer for the real and imaginary parts of the eigenvalues. For $k_z \leqslant k_0$

$$\text{Re}(\Gamma) = \frac{\pi \gamma n_0}{k_0} J_n^2\left(\sqrt{k_0^2 - k_z^2}R\right),$$

(40)

$$\text{Im}(\Gamma) = \frac{\pi \gamma n_0}{k_0} J_n\left(\sqrt{k_0^2 - k_z^2}R\right)Y_n\left(\sqrt{k_0^2 - k_z^2}R\right),$$

(41)

while for $k_z > k_0$

$$\text{Re}(\Gamma) = 0,$$

(42)

$$\text{Im}(\Gamma) = -\frac{2\gamma n_0}{k_0} I_n\left(\sqrt{k_z^2 - k_0^2}R\right)K_n\left(\sqrt{k_z^2 - k_0^2}R\right).$$

(43)

Equation (42) shows that states with $k_z > k_0$ are trapped. For such states the probability amplitude to find atoms excited evolves as

$$\beta(t, \mathbf{r}) = e^{i[k_z z - \text{Im}(\Gamma)t]}e^{in\varphi},$$

(44)

and atomic excitation propagates along the cylinder without emitting a photon outside the cylinder. States with $k_z > k_0$ never emit a photon in free space and become evanescent waves.

For $k_z \leqslant k_0$ photons can be emitted outside and states decay. Equation (40) shows that the timed-Dicke state (with $n = 0$

and $k_z = k_0$)

$$\beta(\varphi, z) = e^{ik_0 z} \tag{45}$$

has the fastest decay rate:

$$\mathrm{Re}(\Gamma_{\mathrm{TD}}) = \frac{\pi \gamma n_0}{k_0}. \tag{46}$$

However, the collective Lamb shift for such a state logarithmically diverges since $Y_0(x) \approx (2/\pi) \ln(x/2)$ for small x. On the other hand, states for which

$$\sqrt{k_0^2 - k_z^2} R = A_{nl}, \tag{47}$$

where A_{nl} are zeros of the Bessel function $J_n(x)$, are trapped. For such states $\mathrm{Re}(\Gamma) = 0$ and the collective Lamb shift also vanishes: $\mathrm{Im}(\Gamma) = 0$.

As an example, let us consider the state

$$\beta(\varphi, z) = e^{-i \Delta \cdot z} e^{ik_0 z} e^{in\varphi}, \tag{48}$$

where $0 \leqslant \Delta \ll k_0$. If

$$\Delta = \frac{A_{nl}^2}{2k_0 R^2} \tag{49}$$

the state is trapped; however it is superradiant for other values of Δ.

In Fig. 7 we plot the collective decay rate (solid red line) and the frequency shift (dash blue curve) of the axially symmetric state $\beta(\mathbf{r}) = e^{ik_z z}$ as a function of the wave number k_z along the z axis for atoms continuously distributed on the surface of an infinitely long cylinder of radius $k_0 R = 10$. For $k_z > k_0$ the state is trapped and $\mathrm{Re}\,(\Gamma) = 0$. On the other hand, for $k_z \leqslant k_0$ a photon is emitted and the atomic decay rate can be controlled by changing k_z or the radius of the cylinder R.

Next we explore how one can control the collective decay rate by changing the shape of the atomic shell.
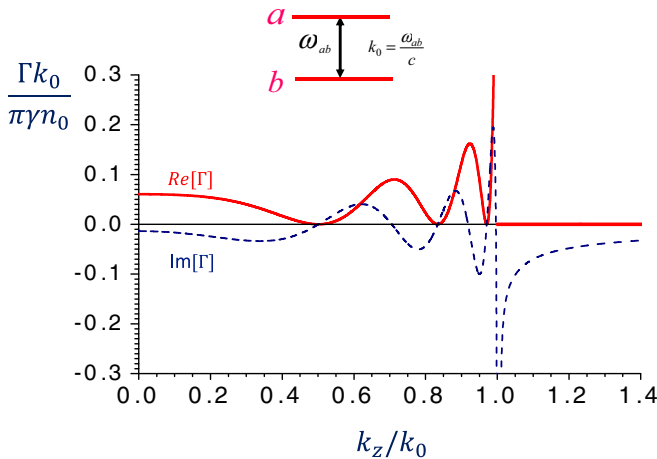

FIG. 7. Collective decay rate (solid red line) and frequency shift (dash blue curve) of the axially symmetric state $\beta(\mathbf{r}) = e^{ik_z z}$ as a function of the wave number k_z along the z axis for atoms continuously distributed on the surface of an infinitely long cylinder of radius $k_0 R = 10$.

IV. SPHEROIDAL SHELL

In this section we consider a general geometry in which N atoms are uniformly distributed on the surface of a spheroidal shell with semiaxes a and b shown in Fig. 1(c). A spheroid, or ellipsoid of revolution, is a surface obtained by rotating an ellipse around one of its principal axes. In Cartesian coordinates x, y, and z, the equation of a spheroid with z as the symmetry axis is given by

$$\frac{x^2 + y^2}{b^2} + \frac{z^2}{a^2} = 1. \tag{50}$$

The semiaxis b is the equatorial radius of the spheroid, and a is the distance from the center to the pole along the symmetry axis. There are two possible cases: $a < b$ (oblate spheroid) and $a > b$ (prolate spheroid). The case of $a = b$ reduces to a sphere.

It is mathematically convenient to adopt the prolate spheroidal coordinates ξ, η, and φ defined by the coordinate transformation with Cartesian coordinates [93]:

$$x = f \sqrt{(\xi^2 - 1)(1 - \eta^2)} \cos \varphi,$$

$$y = f \sqrt{(\xi^2 - 1)(1 - \eta^2)} \sin \varphi,$$

$$z = f \xi \eta,$$

where $f = \sqrt{a^2 - b^2}$, $-1 < \eta < 1$, $\xi \geqslant 1$, and $0 \leqslant \varphi \leqslant 2\pi$. The limits $\xi \to \infty$, $f \to 0$, $f\xi = r$, and $\eta = \cos \theta$ produce spherical polar coordinates.

For $a > b$ the surface $\xi = a/\sqrt{a^2 - b^2}$ forms a prolate spheroid given by Eq. (50). For the spheroidal shell geometry Eq. (3) reads

$$-\frac{i \gamma N}{4\pi} \int_{-1}^{1} d\eta' \int_{0}^{2\pi} d\varphi' \frac{\exp(ik_0 |\mathbf{r} - \mathbf{r}'|)}{k_0 |\mathbf{r} - \mathbf{r}'|} \beta(\eta', \varphi') = \Gamma \beta(\eta, \varphi), \tag{51}$$

where in terms of prolate spheroidal coordinates

$$|\mathbf{r} - \mathbf{r}'| = [(\eta - \eta')^2 a^2 + (2 - \eta^2 - \eta'^2)$$
$$- 2\sqrt{(1 - \eta^2)(1 - \eta'^2)} \cos(\varphi - \varphi')) b^2]^{1/2}. \tag{52}$$

We look for solutions of Eq. (51) in the form

$$\beta(\eta, \varphi) = S_{nm}(k_0 \sqrt{a^2 - b^2}, \eta) e^{im\varphi}, \tag{53}$$

where $S_{nm}(c, \eta)$ are spheroidal angle functions, $n = 0, 1, 2, \ldots$ and $m = -n, -n + 1, \ldots, n - 1, n$. The kernel of the integral equation (51) can be expanded in terms of the spheroidal radial and angle functions as [93]

$$\frac{\exp(ik_0 |\mathbf{r} - \mathbf{r}'|)}{k_0 |\mathbf{r} - \mathbf{r}'|} = \frac{i}{2\pi} \sum_{n=0}^{\infty} \sum_{m=-n}^{n} R_{nm}^{(1)}(k_0 f, \xi) R_{nm}^{(3)}(k_0 f, \xi)$$
$$\times S_{nm}(k_0 f, \eta) S_{nm}(k_0 f, \eta') e^{im(\varphi - \varphi')}, \tag{54}$$

where

$$f = \sqrt{a^2 - b^2},$$

$$\xi = \frac{a}{\sqrt{a^2 - b^2}},$$

and $R_{nm}^{(1)}$ and $R_{nm}^{(3)}$ are spheroidal radial functions of the first and the third kind. Spheroidal angle and radial functions are generalizations of Legendre functions and spherical Bessel functions for spheroidal coordinates rather than for the spherical polar coordinates in which the latter functions usually occur. The spheroidal radial function $R_{nm}^{(1)}(c,\xi)$ becomes a spherical Bessel function in the limit of zero c, while $R_{nm}^{(3)}(c,\xi)$ becomes a spherical Hankel function. The transition to the oblate spheroid ($a < b$) is obtained by replacing $\sqrt{a^2 - b^2}$ with $i\sqrt{b^2 - a^2}$. Spheroidal functions occur in many contexts; e.g., they are used to describe scattering by nonspherical nuclei, wave functions of diatomic molecules, analysis of band-limited random noise, and anisotropy of the cosmic microwave background radiation.

The derivation of eigenfunctions of Eq. (51) is similar to the case of the spherical shell. Using the orthogonality condition for spheroidal angle functions

$$\int_{-1}^{1} d\eta\, S_{nm}(c,\eta) S_{n'm}(c,\eta) = \delta_{nn'} \tag{55}$$

and Eq. (37), we find the following answer for eigenvalues:

$$\Gamma_{nm} = N\gamma\, R_{nm}^{(1)}(k_0 f,\xi) R_{nm}^{(3)}(k_0 f,\xi). \tag{56}$$

Taking into account that

$$R_{nm}^{(3)}(c,\xi) = R_{nm}^{(1)}(c,\xi) + i R_{nm}^{(2)}(c,\xi),$$

where $R_{nm}^{(2)}(c,\xi)$ is the spheroidal radial function of the second kind, we obtain that real and imaginary parts of the eigenvalues are given by

$$\mathrm{Re}(\Gamma_{nm}) = N\gamma \left[R_{nm}^{(1)}(k_0 f,\xi) \right]^2, \tag{57}$$

$$\mathrm{Im}(\Gamma_{nm}) = N\gamma\, R_{nm}^{(1)}(k_0 f,\xi) R_{nm}^{(2)}(k_0 f,\xi). \tag{58}$$

For $a < b$ we should replace $\sqrt{a^2 - b^2}$ with $i\sqrt{b^2 - a^2}$, that is, $\xi \to i\xi$. Spheroidal functions $R_{nm}^{(1)}$ and $R_{nm}^{(2)}$ remain real-valued despite this replacement. Equations (57) and (58) allow
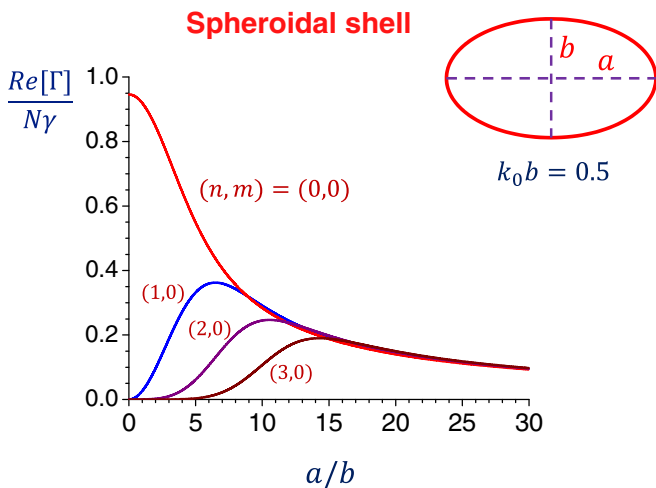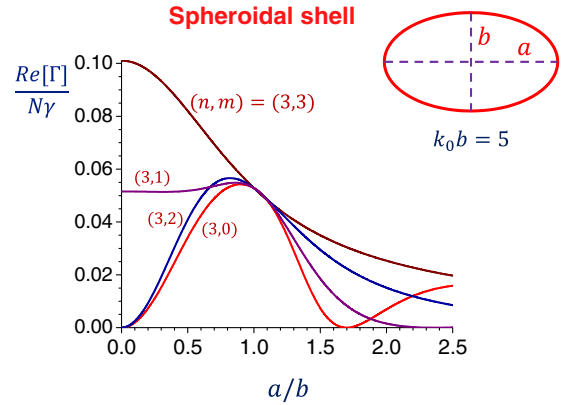
FIG. 9. Collective decay rate of eigenstates of a spheroidal shell with quantum numbers $(n,m) = (3,0)$, $(3,1)$, $(3,2)$, and $(3,3)$ as a function of the axes' length ratio a/b. Length b is fixed such that $k_0 b = 5$.

us to investigate crossover between spherical and cylindrical geometries and study how the shape of the atomic shell affects the collective emission of the photon.

Next we discuss several interesting examples. In Fig. 8 we plot the collective decay rate of eigenstates of a spheroidal shell with quantum numbers $(n,m) = (0,0)$, $(1,0)$, $(2,0)$, and $(3,0)$ as a function of the axes' length ratio a/b. We assume that the spheroidal shell has semiaxes a (axis of revolution) and b and the length of b is fixed such that $k_0 b = 0.5$. When $a \ll b$, we are in the small sample limit in which the symmetric state $(0,0)$ is superradiant and other states are trapped. If we start to stretch the spheroidal shell along the a axis (increase a) the trapped states become superradiant and their decay rates merge with the decay rate of the $(0,0)$ state.

Figure 9 shows the collective decay rate of eigenstates of a spheroidal shell with quantum numbers $(n,m) = (3,0)$, $(3,1)$, $(3,2)$, and $(3,3)$ as a function of the axes' length ratio a/b. We assume that length b is fixed such that $k_0 b = 5$. If $a = b$ (spherical shell) the states are degenerate. However, if we

FIG. 8. Collective decay rate of eigenstates of a spheroidal shell with quantum numbers $(n,m) = (0,0)$, $(1,0)$, $(2,0)$, and $(3,0)$ as a function of the axes' length ratio a/b. Length b is fixed such that $k_0 b = 0.5$.
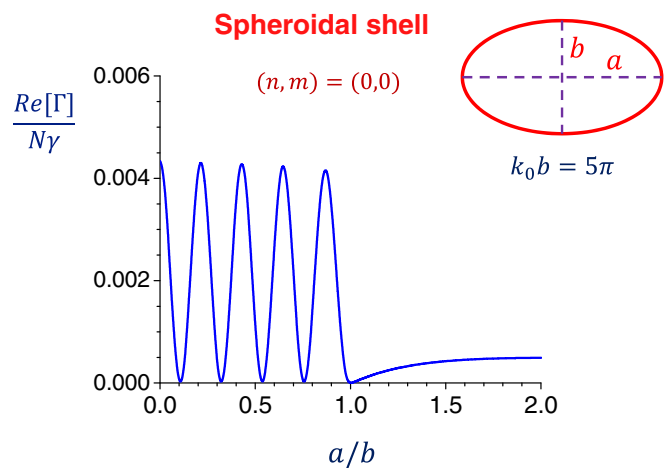
FIG. 10. Collective decay rate of eigenstates of a spheroidal shell with quantum numbers $(n,m) = (0,0)$ as a function of the axes' length ratio a/b. Length b is fixed such that $k_0 b = 5\pi$.

deform the sphere the degeneracy is lifted and states start to evolve with different decay rates.

Finally, in Fig. 10 we plot the collective decay rate of an eigenstate of a spheroidal shell with quantum numbers $(n,m) = (0,0)$ as a function of the axes' length ratio a/b. We assume that length b is fixed at a special value of $k_0 b = 5\pi$. If $a = b$ such a state is trapped (the collective decay rate vanishes). However, if we compress the sphere along the a-axis (decrease a) the state's decay rate oscillates between zero and a maximum value. Thus, by changing shape of the spheroid we can manipulate the state dynamics between superradiant emission and trapping of atomic excitation.

V. CONCLUSION

Cooperative spontaneous emission of a single photon by atomic ensemble is an interesting physics which combines virtual transitions and the Lamb shift with many-particle effects. The collective nature of photon emission can result in radiation speed up or light trapping. Total suppression of spontaneous decay can occur for certain atomic geometries despite the presence of virtual transitions. A change in the shape of the atomic system or its size can yield superradiant decay of the otherwise trapped state. Such a property could be useful for quantum information storage and the design of optical switches.

In this paper we found eigenstates and their collective decay rates and frequency shifts for two-dimensional atomic structures of various shapes. Such two-dimensional structures can be made by bombarding crystals with atomic beams and creating defects at the sample surface. Nitrogen vacancy centers on the surface of diamonds is an example of shell-like two-dimensional configurations. Preparation of various collective atomic states in shell-like structures is substantially easier than that for bulk atomic samples for which resonant photons get absorbed in a thin layer near the sample surface.

It is remarkable that eigenstates for spherical, cylindrical, and spheroidal atomic shells that we study can be obtained analytically even when virtual processes are included. This is usually not the case for bulk atomic samples. Our exact solutions provide useful insight on the problem of collective atomic emission by showing precisely how the shape and the size of the shell influence dynamics of the photon emission. They can help us to design atomic structures with the desired properties, e.g., superradiant or light-trapping configurations. Our solution for spheroidal shells also demonstrates how collective atomic emission changes during transition between spherical and cylindrical geometries.

ACKNOWLEDGMENTS

[1] R. Dicke, Phys. Rev. **93**, 99 (1954).

[2] J. P. Dowling, Found. Phys. **23**, 895 (1993).

[3] V. V. Datsyuk, JETP Lett. **75**, 368 (2002).

[4] H. T. Dung and K. Ujihara, Phys. Rev. A **60**, 4067 (1999).

[5] M. M. Dignam, D. P. Fussell, M. J. Steel, C. M. de Sterke and R. C. McPhedran, Phys. Rev. Lett. **96**, 103902 (2006).

[6] A. Auffeves, D. Gerace, S. Portolan, A. Drezet, and M. F. Santos, New J. Phys. **13**, 093020 (2011).

[7] W. E. Lamb and R. C. Retherford, Phys. Rev. **72**, 241 (1947).

[8] C. Cohen-Tannoudji, J. Dupont-Roc, and G. Grynberg, *Photons and Atoms: Introduction to Quantum Electrodynamics* (Wiley & Sons, New York, 1997).

[9] S. De Liberato, D. Gerace, I. Carusotto, and C. Ciuti, Phys. Rev. A **80**, 053810 (2009).

[10] A. A. Svidzinsky and M. O. Scully, Opt. Commun. **282**, 2894 (2009).

[11] R. Friedberg and J. T. Manassah, Laser Phys. **20**, 250 (2010).

[12] A. A. Svidzinsky, J.-T. Chang, and M. O. Scully, Phys. Rev. A **81**, 053821 (2010).

[13] R. Friedberg, S. R. Hartmann, and J. T. Manassah, Phys. Rep. **7**, 101 (1973).

[14] M. O. Scully, Phys. Rev. Lett. **102**, 143601 (2009).

[15] R. Friedberg and J. T. Manassah, Phys. Lett. A **373**, 3423 (2009).

[16] R. Röhlsberger, K. Schlage, B. Sahoo, S. Couet, and R. Rüffer, Science **328**, 1248 (2010).

[17] M. O. Scully and A. A. Svidzinsky, Science **328**, 1239 (2010).

[18] R. Friedberg and J. T. Manassah, Phys. Rev. A **81**, 063822 (2010).

[19] J. Keaveney, A. Sargsyan, U. Krohn, I. G. Hughes, D. Sarkisyan, and C. S. Adams, Phys. Rev. Lett. **108**, 173601 (2012).

[20] D. C. Burnham and R. Y. Chiao, Phys. Rev. **188**, 667 (1969).

[21] A. A. Svidzinsky, J.-T. Chang, and M. O. Scully, Phys. Rev. Lett. **100**, 160504 (2008).

[22] A. A. Svidzinsky, L. Yuan, and M. O. Scully, Phys. Rev. X **3**, 041001 (2013).

[23] N. Skribanowitz, I. P. Herman, J. C. MacGillivray, and M. S. Feld, Phys. Rev. Lett. **30**, 309 (1973).

[24] H. Xia, A. A. Svidzinsky, L. Yuan, C. Lu, S. Suckewer, and M. O. Scully, Phys. Rev. Lett. **109**, 093604 (2012).

[25] A. Goban, C.-L. Hung, J. D. Hood, S.-P. Yu, J. A. Muniz, O. Painter, and H. J. Kimble, Phys. Rev. Lett. **115**, 063601 (2015).

[26] E. Hanamura, Phys. Rev. B **38**, 1228 (1988).

[27] J. Knoester, Phys. Rev. Lett. **68**, 654 (1992).

[28] G. Björk, S. Pau, J. M. Jacobson, H. Cao, and Y. Yamamoto, Phys. Rev. B **52**, 17310 (1995).

[29] V. M. Agranovich, D. M. Basko, and O. A. Dubovsky, J. Chem. Phys. **106**, 3896 (1997).

[30] T. Takagahara, Phys. Rev. B **47**, 16639(R) (1993).

[31] H. Ajiki, T. Tsuji, K. Kawano, and K. Cho, Phys. Rev. B **66**, 245322 (2002).

[32] C. Creatore and A. L. Ivanov, Phys. Rev. B **77**, 075324 (2008).

[33] M. Bamba and H. Ishihara, Phys. Rev. B **80**, 125319 (2009).

[34] T. Itoh, T. Ikehara, and Y. Iwabuchi, J. Lumin. **45**, 29 (1990).

[35] M. O. Scully, E. S. Fry, C. H. R. Ooi, and K. Wodkiewicz, Phys. Rev. Lett. **96**, 010501 (2006).

[36] J. Eberly, J. Phys. B: At., Mol. Opt. Phys. **39**, S599 (2006).

[37] I. E. Mazets and G. Kurizki, J. Phys. B: At., Mol. Opt. Phys. **40**, F105 (2007).

[38] A. Svidzinsky and J.-T. Chang, Phys. Rev. A **77**, 043833 (2008).

[39] R. Friedberg and J. T. Manassah, Phys. Lett. A **372**, 2514 (2008).

[40] R. Friedberg and J. T. Manassah, Phys. Lett. A **372**, 2787 (2008).

[41] R. Friedberg and J. T. Manassah, Opt. Commun. **281**, 4391 (2008).

[42] R. Friedberg and J. T. Manassah, Phys. Lett. A **372**, 6833 (2008).

[43] D. Porras and J. I. Cirac, Phys. Rev. A **78**, 053816 (2008).

[44] S. Das, G. S. Agarwal, and M. O. Scully, Phys. Rev. Lett. **101**, 153601 (2008).

[45] M. O. Scully and A. A. Svidzinsky, Science **325**, 1510 (2009).

[46] M. O. Scully and A. A. Svidzinsky, Phys. Lett. A **373**, 1283 (2009).

[47] L. H. Pedersen and K. Mølmer, Phys. Rev. A **79**, 012320 (2009).

[48] B. G. Kim, C. H. R. Ooi, M. Ikram, and H. W. Lee, Phys. Lett. A **373**, 1658 (2009).

[49] J. T. Manassah, Laser Phys. **19**, 2102 (2009).

[50] R. Friedberg, Ann. Phys. **325**, 345 (2010).

[51] S. Prasad and R. J. Glauber, Phys. Rev. A **82**, 063805 (2010).

[52] E. M. Kessler, S. Yelin, M. D. Lukin, J. I. Cirac, and G. Giedke, Phys. Rev. Lett. **104**, 143601 (2010).

[53] R. Wiegner, J. von Zanthier, and G. S. Agarwal, Phys. Rev. A **84**, 023805 (2011).

[54] P. R. Berman and J.-L. Le Gouet, Phys. Rev. A **83**, 035804 (2011).

[55] R. Friedberg, J. Phys. B: At., Mol. Opt. Phys. **44**, 175505 (2011).

[56] T. Bienaimé, N. Piovella, and R. Kaiser, Phys. Rev. Lett. **108**, 123602 (2012).

[57] A. A. Svidzinsky, Phys. Rev. A **85**, 013821 (2012).

[58] Y. Li, J. Evers, H. Zheng, and S.-Y. Zhu, Phys. Rev. A **85**, 053830 (2012).

[59] T. Bienaimé, R. Bachelard, N. Piovella, and R. Kaiser, Fortschr. Phys. **61**, 377 (2013).

[60] Y. Miroshnychenko, U. V. Poulsen, and K. Molmer, Phys. Rev. A **87**, 023821 (2013).

[61] Yong Li, Jörg Evers, W. Feng, and S.-Y. Zhu, Phys. Rev. A **87**, 053837 (2013).

[62] G. Y. Slepyan and A. Boag, Phys. Rev. Lett. **111**, 023602 (2013).

[63] N. Piovella, R. Bachelard, and Ph. W. Courteille, J. Plasma Phys. **79**, 413 (2013).

[64] U. van Bürck, D. P. Siddons, J. B. Hastings, U. Bergmann, and R. Hollatz, Phys. Rev. B **46**, 6207 (1992).

[65] Y. Kagan, Hyperfine Interact. **123/124**, 83 (1999).

[66] G. T. Trammell and J. P. Hannon, Phys. Rev. B **18**, 165 (1978).

[67] H. J. Lipkin, Phys. Rev. Lett. **58**, 1176 (1987).

[68] B. W. Adams, J. Mod. Opt. **56**, 1974 (2009).

[69] R. Röhlsberger, Fortschr. Phys. **61**, 360 (2013).

[70] A. A. Svidzinsky, X. Zhang, and M. O. Scully, Phys. Rev. A **92**, 013801 (2015).

[71] L.-M. Duan, M. D. Lukin, J. I. Cirac, and P. Zoller, Nature (London) **414**, 413 (2001).

[72] C. H. van der Wal, M. D. Eisaman, A. André, R. L. Walsworth, D. F. Phillips, A. S. Zibrov, and M. D. Lukin, Science **301**, 196 (2003).

[73] A. Kuzmich, W. P. Bowen, A. D. Boozer, A. Boca, C. W. Chou, L.-M. Duan, and H. J. Kimble, Nature (London) **423**, 731 (2003).

[74] M. D. Eisaman, L. Childress, A. André, F. Massou, A. S. Zibrov, and M. D. Lukin, Phys. Rev. Lett. **93**, 233602 (2004).

[75] B. Casabone, K. Friebe, B. Brandstätter, K. Schüppert, R. Blatt, and T. E. Northup, Phys. Rev. Lett. **114**, 023602 (2015).

[76] R. Reimann, W. Alt, T. Kampschulte, T. Macha, L. Ratschbacher, N. Thau, S. Yoon, and D. Meschede, Phys. Rev. Lett. **114**, 023601 (2015).

[77] M. O. Scully, Phys. Rev. Lett. **115**, 243602 (2015).

[78] A. Kalachev and S. Kroll, Phys. Rev. A **74**, 023814 (2006).

[79] A. Kalachev, Phys. Rev. A **76**, 043812 (2007).

[80] M. D. Eisaman, A. Andre, F. Massou, M. Fleischhauer, A. S. Zibrov, and M. D. Lukin, Nature (London) **438**, 837 (2005).

[81] C. W. Chou, S. V. Polyakov, A. Kuzmich, and H. J. Kimble, Phys. Rev. Lett. **92**, 213601 (2004).

[82] A. T. Black, J. K. Thompson, and V. Vuletic, Phys. Rev. Lett. **95**, 133601 (2005).

[83] H. W. Chan, A. T. Black, and V. Vuletic, Phys. Rev. Lett. **90**, 063003 (2003).

[84] M. Wolke, J. Klinner, H. Kessler, and A. Hemmerich, Science **337**, 75 (2012).

[85] J. G. Bohnet, Z. Chen, J. M. Weiner, D. Meiser, M. J. Holland, and J. K. Thompson, Nature (London) **484**, 78 (2012).

[86] X. Zhang and A. A. Svidzinsky, Phys. Rev. A **88**, 033854 (2013).

[87] V. Ernst, Z. Phys. **218**, 111 (1969).

[88] J. T. Manassah, Phys. Rev. A **82**, 053816 (2010).

[89] A. A. Svidzinsky, Opt. Commun. **284**, 269 (2011).

[90] R. Friedberg and J. T. Manassah, J. Math. Phys. **52**, 042107 (2011).

[91] R. Friedberg and J. T. Manassah, Phys. Lett. A **372**, 4164 (2008).

[92] H. Ajiki, T. Kaneno, and H. Ishihara, Phys. Rev. B **73**, 155322 (2006).

[93] C. Flammer, *Spheroidal Wave Functions* (Stanford University Press, Stanford, CA, 1957).